Laser-generated thermoelastic acoustic sources in anisotropic materials

David H. Hurley[a)]
Idaho National Engineering and Environmental Laboratory, P.O. Box 1625, Idaho Falls, Idaho 83415-2209

(Received 15 December 2003; revised 27 January 2004; accepted 4 February 2004)

An analytical model appropriate for thermoelastic generation of acoustic waves in anisotropic materials is presented for both plane and line sources. The interaction of acoustic waves produced by subsurface sources with the bounding surface is accounted for using a method of images. For the plane source case, analytical solutions are found that form an appropriate basis for an angular spectrum of plane waves. For the line source case and for specific crystal symmetries and source orientations, it is shown in the limit of strong optical absorption, a buried line source is equivalent to applying a shear stress dipole at the bounding surface. However, contrary to the isotropic case, the character and strength of the equivalent surface stress is a function of propagation direction. © *2004 Acoustical Society of America.* [DOI: 10.1121/1.1690080]

PACS numbers: 43.35.Sx [YHB] Pages: 2054–2058

I. INTRODUCTION

Since the early 1960s there has been considerable interest in generating acoustic waves using pulsed laser irradiation. The early experimental work in this field used low repetition rate (10 Hz) Q-switched lasers with nanosecond pulse lengths for acoustic generation (nanosecond laser acoustics).[1–3] A large part of the modeling effort for nanosecond laser acoustics has relied on replacing the laser source with an equivalent set of stress boundary conditions.[2,4] This equivalent stress distribution, which takes the form of a shear stress dipole for isotropic material, has proven to be extremely useful in describing many features of laser generated (thermoelastic regime) acoustic waveforms. For instance, the epicental waveform,[5,6] the surface acoustic waveform,[7] and the displacement directivity pattern[8,9] are all modeled accurately using a set of stress boundary conditions that are equivalent to a thermoelastic source in the limit of strong optical absorption.

In the mid-1980s a second type of pulsed laser acoustics emerged that used high repetition rate ($\sim$80 MHz) ultrafast laser pulses ($\sim$100 fs) to generate and detect acoustic pulses with pulse durations of a few picoseconds.[10] The temporal-resolution-afforded picosecond acoustics has enabled researchers to concentrate on relating the source characteristics to fundamental physical processes.[11–13] The modeling effort for picosecond acoustics typically involves 1-D models that exploit the simple experimental geometry.[14]

For nanosecond acoustics, work specific to laser sources in anisotropic materials has been reported by Every and Sachse.[15] In their work, data interpretation concentrated on wavefront analysis. By contrast, Mourad *et al.*,[16] used the Cagniard–deHoop[17] method to obtain numerically the solutions for laser excitation in an anisotropic half-space where it was assumed, in analogy to the isotropic case, that the laser source could be modeled as a shear stress dipole applied at the material surface. In a similar approach Hurley and Spicer[18] developed analytical solutions for thermoelastic generation in transversely isotropic materials by a laser line and laser point source.

For picosecond acoustics, work specific to elastically anisotropic materials has been primarily experimental in nature and typically involves acoustic propagation in high symmetry directions.[19–22] Recently, Hurley *et al.*[23] have reported generation of picosecond shear waves using an ultrafast pump probe method. This study involved laser generation of longitudinal waves in an isotropic aluminum film. A portion of the longitudinal wave was mode converted to a shear wave at the interface between the isotropic film and anisotropic substrate. The shear acoustic waves were detected using an off-axis polarization sensitive detection scheme.

In this article both plane (1-D problem geometry) and line (2-D problem geometry) thermoelastic sources, appropriate for picosecond and nanosecond laser acoustics in elastically anisotropic half-spaces, are examined in detail using a method of images to satisfy the stress boundary conditions. The method of images in general involves finding the solution to a particular boundary-value-problem by introducing a fictitious source (image source) in a boundless medium that together with the actual source satisfies the boundary conditions. This method, which is employed routinely for electrostatic problems, does not find the same popularity in dynamic elasticity since, for typical applications, satisfying both the shear stress and normal stress conditions at the boundary is not possible.[24] For the 1-D case considered in this manuscript, the method of images is applied in a very straightforward manner enabling an analytical solution for the displacements. In the 2-D case, a hybrid version of the method of images is used to obtain an equivalent set of stress boundary conditions for a limited set of crystal symmetries/line-source orientations.

II. THEORETICAL DEVELOPMENT

The following equations provide a general description of thermoelastic generation in anisotropic materials (strain rate coupling has been neglected):

[a)]Electronic mail: hurldh@inel.gov

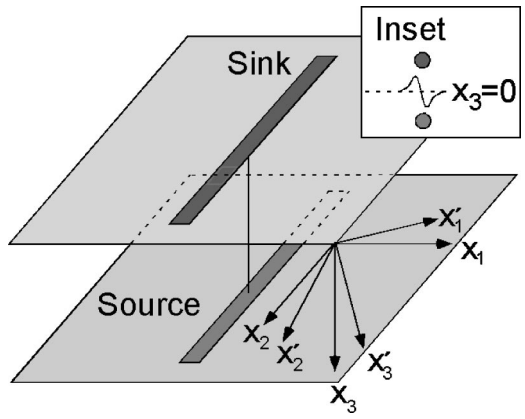

FIG. 1. Source/sink specifications. The axis/plane of the line/plane source/sink is perpendicular to the x_3 axis and parallel with the x_2 axis. The separation plane is perpendicular to the x_3 axis and is midway between the source and sink. The crystal axes coincide with the prime coordinate system. Inset: Conceptual illustration of the shear stress distribution at the separation plane resulting from the source/sink combination for the 2-D case.

$$\kappa'_{ij}T_{,ij}-\rho CT_{,t}+Q=0, \quad C'_{ijkl}u_{l,kj}-\rho u_{i,tt}=\beta'_{ij}T_{,j}. \tag{1}$$

The first equation is the linearized heat conduction equation and the second is the equation of motion for a linear elastic material. The material constants, κ'_{ij}, β'_{ij}, C'_{ijkl}, ρ, and C, are defined as the thermal conductivity tensor, the thermal pressure tensor, the elastic stiffness tensor, the mass density, and the specific heat respectively. The components of displacement and temperature are defined as u_i and T. In this development the crystal axes, which coincide with the prime coordinate system, have an arbitrary orientation relative to the unprimed axes (Fig. 1). The crystalline symmetry as it relates to the various tensor symmetries will be discussed in detail in the following sections. Since strain-rate coupling has been neglected, the solution to the heat conduction equations can be sought without considering the elastic equations of motion. Given that the spirit of this article is to provide analytical insight into the role of elastic and thermal anisotropy in thermoelastic generation of acoustic waves, heat diffusion will be neglected.[4,25] The temperature fields for both the 1-D and 2-D case are found by taking the temporal integral of the absorbed laser energy (q_0):

$$\begin{aligned} T_{1\text{-}D}&=T_0H(t)[\,\delta(x_3-a)-\delta(x_3+a)\,],\\ T_{2\text{-}D}&=T_0H(t)\,\delta(x_1)[\,\delta(x_3-a)-\delta(x_3+a)\,], \end{aligned} \tag{2}$$

where $T_0=q_0/\rho C$. The source, which is concentrated a distance $+a$ from the surface, is associated with an increase in temperature and the image source (sink), which is concentrated a distance $-a$ from the surface, is associated with a decrease in temperature (Fig. 1).[26] The solution procedure for the elastic displacements for the 1-D and 2-D cases involves applying a Fourier/Laplace transform to remove dependence on the spatial and temporal variables:

$$\begin{aligned} F(\eta,\kappa,s)=\frac{1}{2\pi}\int_{-\infty}^{\infty}\int_{-\infty}^{\infty}\int_{0}^{\infty}f(x_1,x_3,t)\\ \times e^{(i\eta x_1+i\kappa x_3-st)}dtdx_1dx_3. \end{aligned} \tag{3}$$

For the 1-D case the solution depends only on x_3 while the 2-D case depends on both x_1 and x_3. The transformed equations take the form

$$N\cdot\overline{u}=S, \tag{4}$$

where barred quantities refer to transformed variables and N and S which are functions of the transform parameters are define in the Appendix. The transformed displacements are decoupled algebraically giving

$$\begin{aligned} &\overline{u_i}=\frac{D_i}{D_0}, \quad D_1=\det(N_1),\\ &D_0=\det(N)=d_0(\kappa^2-\kappa_1^2)(\kappa^2-\kappa_2^2)(\kappa^2-\kappa_3^2), \end{aligned} \tag{5}$$

where N_i is obtained from N by replacing the ith column with S and κ_i are the roots of D_0. Using partial fractions the transformed displacements may be represented as

$$\begin{aligned} &\overline{u_i}=\sum_{j=1}^{3}\frac{A_{ij}}{d_0(\kappa^2-\kappa_j^2)}, \quad A_{ij}=\frac{D_i(\kappa_j)}{(\kappa_j-\kappa_{r1})(\kappa_j-\kappa_{r2})},\\ &r_1\neq j, \ \ r_2\neq j, \ \ r_2\neq r_1, \end{aligned} \tag{6}$$

where the amplitude coefficients, A_{ij}, are functions of propagation direction for elastically anisotropic materials.

A. One-dimensional case

The Fourier inversion now may be written as

$$\begin{aligned} &\overline{u_i}(x_3,s)=\frac{-\overline{A}_{ij}}{d_0}\sqrt{\frac{2}{\pi}}\frac{\partial}{\partial x_3}\left[\,\mathrm{Re}\int_0^{\infty}\frac{E(\omega,s,x_3)}{s^2(\omega^2-\omega_j^2)}d\omega\right],\\ &\overline{A}_{ij}=\frac{A_{ij}}{i\omega E(\omega,s,x_3)},\\ &E(\omega,s,x_3)=(e^{-i\omega s|x_3-a|}-e^{-i\omega s|x_3+a|}), \end{aligned} \tag{7}$$

where the substitution, $\kappa=s\omega$, has been made to facilitate the transform inversion.[27] The real ω axis is identified as the Fourier inversion path and the imaginary ω axis is identified as the Cagniard path.[17,28,29] Since all the poles lie on the imaginary ω axis, the Fourier inversion is accomplished by summing the residues along the imaginary ω axis:

$$\begin{aligned} \int_0^{\infty}\frac{E(\omega,s,x_3)}{(\omega^2-\omega_j^2)}d\omega&=\pi i\,\mathrm{Res}\left\{\frac{E(\omega,s,x_3)}{(\omega^2-\omega_j^2)}\right\}\\ &=\cdots\pi i\left(\frac{E(\omega_j,s,x_3)}{2\omega_j}\right). \end{aligned} \tag{8}$$

Given that the dependence on x_3 has been recovered, the stresses at the separation plane ($x_3=0$) can be evaluated:

$$\sigma_{3j}=C'_{3j13}u_{1,3}+C'_{3j23}u_{2,3}+C'_{3j33}u_{3,3}=0. \tag{9}$$

A detailed analysis of the stress can be circumvented by noting that the displacements are of the form

$$u_i\propto\frac{\partial^2}{\partial x_3^2}(e^{-\overline{\omega s}|x_3-a|}-e^{-\overline{\omega s}|x_3+a|}). \tag{10}$$

Since the displacement components are even functions about the plane $x_3=0$, it follows that the stresses at the separation

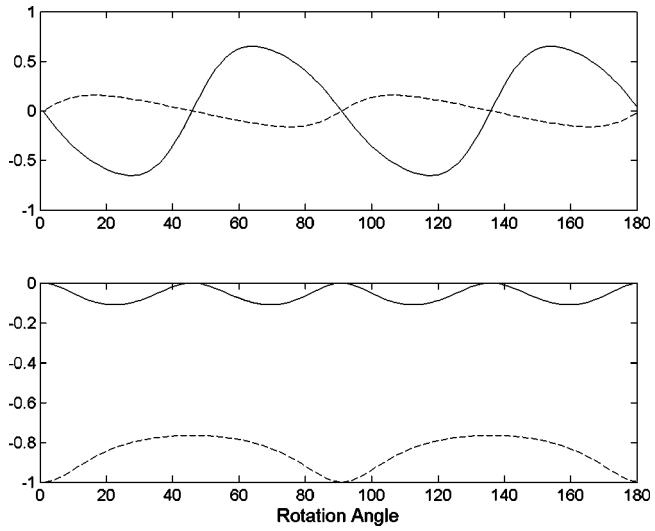

FIG. 2. Amplitude coefficients versus rotation about the x_2 axis [values have been normalized using $\overline{A}_{33}(\theta=0)$]. Top: solid line corresponds to normalized $\overline{A}_{11}$ [i.e., $G_{11}/G_{33}(\theta=0)$] and bottom line corresponds to normalized $\overline{A}_{13}$ [i.e., $G_{11}/G_{33}(\theta=0)$]. Bottom: solid and dashed line correspond to normalized $\overline{A}_{31}$ and $\overline{A}_{33}$, respectively.

plane must be zero. Thus for the 1-D case, a source and image sink satisfy stress free conditions at $x_3=0$ and, hence, the separation plane can be identified with the bounding plane of an elastic half-space. Furthermore, this combination of thermoelastic source and image sink in an unbounded medium is equivalent to a thermoelastic source in an elastic half-space. Since the image sink produces a modal amplitude distribution that is of equal magnitude and opposite sign to that of the source, mode converted waves are not required to satisfy the stress-free boundary conditions. This, however, is not the case for the somewhat similar problem of two half-spaces having different orientations.[23,30] Dependence on time is recovered using a table of Laplace transform-pairs giving

$$u_i(x_3,t)=\sqrt{\frac{\pi\overline{A}_{ij}^2}{2d_0^2}}\left\{\begin{array}{l} H(x_3-a)H(t-\overline{\omega}_j(x_3+a))\cdots \\ -H(a-x_3)H(t+\overline{\omega}_j(x_3+a)) \\ -H(x_3+a)H(t-\overline{\omega}_j(x_3-a))\cdots \\ +H(-x_3-a)H(t+\overline{\omega}_j(x_3-a)) \end{array}\right\}. \tag{11}$$

As a check on the solution, it can be shown that the eigenvectors corresponding to the homogeneous solution can be formed from appropriate ratios of amplitude coefficients, A_{ij}. However, contrary to the homogeneous solution, the displacement waveforms given in Eqs. (11) form an appropriate bases for an angular spectrum of planes waves which could be used in the calculation of acoustic diffraction resulting from 2-D and 3-D thermal sources.[31]

To elucidate the effect of elastic anisotropy on the source strength, consider a material with cubic symmetry for which the amplitude coefficient can be separated into two terms:

$$\overline{A}_{ij}=T_0\beta_0 G_{ij}, \tag{12}$$

where β_0 is a function of both elastic and thermal constants[32] and G_{ij}, which is a function of only the elastic constants, gives the variation of the displacement amplitudes with propagation direction. The strong dependence of G_{ij} on propagation direction is illustrated in Fig. 2. The material constants are for single crystal Cu (cubic) and the initial orientation corresponds to the prime axes coinciding with the unprime axes. The solution is solved repetitively as the sample is rotated about the x_2 axis.

B. Two-dimensional case

For a two-dimensional source, analytical solutions exist only for certain crystal symmetries and for certain source/observation orientations.[7,18] However, instead of finding expressions for the displacements, the emphasis of this section will be on prescribing a set of stress boundary conditions that is equivalent to a center of thermal expansion located at the bounding surface.[33] Much of the groundwork has already been done in the previous section. The symmetries/orientations that will be discussed are given in Table I and correspond to cases for which D_0 can be split into two parts, one of second order and one of forth order in κ. Physically this corresponds to waves that are polarized in the (x_1,x_3) plane. Performing the same mathematical manipulations given in the preceding section, the displacements can be represented as

$$\begin{aligned} \overline{u}_1(\eta,\kappa,s)&=\frac{-i\eta\overline{A}_{1j}}{d_0}\frac{E(\kappa)}{\kappa^2-\kappa_j^2}, \\ \overline{u}_3(\eta,\kappa,s)&=\frac{-i\kappa\overline{A}_{3j}}{d_0}\frac{E(\kappa)}{\kappa^2-\kappa_j^2}, \\ E(\kappa)&=e^{ia\kappa}-e^{-ia\kappa}. \end{aligned} \tag{13}$$

Dependence on x_3 is regained using a table of transform pairs and is given as

$$\begin{aligned} \overline{u}_1(\eta,x_3,s)&=-\sqrt{\frac{\pi}{2}}\frac{i\eta\overline{A}_{1j}}{d_0\kappa_j}E(\kappa_j,x_3), \\ \overline{u}_3(\eta,x_3,s)&=\sqrt{\frac{\pi}{2}}\frac{\overline{A}_{3j}}{d_0\kappa_j}\frac{\partial E(\kappa_j,x_3)}{\partial x_3}, \\ E(\kappa_j)&=e^{-\kappa_j|x_3-a|}-e^{-\kappa_j|x_3+a|}. \end{aligned} \tag{14}$$

The next step in the process is to evaluate the stresses at the separation plane. Applying both a Laplace and Fourier transform to eliminate dependence on x_1 and time, the transformed stresses at the separation plane for all the cases excluding case 4 in Table I are represented as

$$\begin{aligned} \overline{\sigma}_{13}(\eta,x_3,s)&=-i\eta C'_{55}\overline{u}_3+C'_{55}\overline{u}_{1,3}, \\ \overline{\sigma}_{33}(\eta,x_3,s)&=-i\eta C'_{13}\overline{u}_1+C'_{33}\overline{u}_{3,3}. \end{aligned} \tag{15}$$

By noting that $\overline{u}_1$ and $\overline{u}_{3,3}$ are both odd functions of x_3, the normal stress evaluated at the separation plane is necessarily zero. However, the shear stress, σ_{13}, is nonzero at the separation plane. If, in addition to the source/sink combination, a shear stress of opposite sign and equal magnitude is applied at the separation plane, a stress free state is achieved at the separation plane (Fig. 1 inset). Thus the combination of (1) source, (2) sink and (3) shear stress applied at the

TABLE I. The seven crystal symmetries/line-source orientations considered. Crystalographic axes are defined as X, Y, Z and $R45°(x_1)$ refers to a 45° rotation about the x_1 axis. Cases 1–3 and 5–7 give the strength of the shear stress dipole, Γ_{13}, in terms of the elastic constants in the nonrotated frame (i.e., the crystallographic axes coincide with the unprimed axes).

Structure	Cubic (1)	Cubic (2)	Cubic (3a,3b)	Cubic (4)
Orientation	$R45°(x_1)$ $x_1 \| X$	$R45°(x_2)$ $x_2 \| Y$	(a) $R45°(x_3)$ $x_3 \| Z$ (b) $x_1, x_2, x_3 \| XYZ$	$R\theta(x_2), x_1 \| X, x_2 \| Y$
Γ_{13}/β_0	$\frac{C_{11}+2C_{44}-C_{12}}{C_{11}+C_{12}+2C_{44}}$	$\frac{4C_{44}}{C_{11}+C_{12}+2C_{44}}$	$\frac{C_{11}-C_{12}}{C_{11}}$	N/A
Structure	Hexagonal (5)	Tetragonal (6)	Orthorhombic (7)	
Orientation	$x_3 \| Z$	$x_1, x_2, x_3 \| XYZ$	$x_1, x_2, x_3 \| XYZ$	
Γ_{13}	$\frac{\beta_{11}C_{33}-\beta_{33}C_{13}}{C_{33}}$	$\frac{\beta_{11}C_{33}-\beta_{33}C_{13}}{C_{33}}$	$\frac{\beta_{11}C_{33}-\beta_{33}C_{13}}{C_{33}}$	

separation plane is equivalent to a source in an elastic half-space. At this point inverting the shear stress would be difficult if not impossible analytically. However, if the source and sink are brought together at the separation plane, they necessarily annihilate, leaving a very simple expression for the applied shear stress:

$$\overline{\sigma}_{13}(\eta, x_3=0, s) = \frac{-i\eta}{s\sqrt{2\pi}} T_0 \Gamma_{13},$$

$$\sigma_{13}(x_1, x_3=0, s) = T_0 \Gamma_{13} H(t) \frac{\partial \delta(x_1)}{\partial x_1}. \tag{16}$$

The functional form of the equivalent surface shear stress is a dipole, similar to the expression given by Rose.[4] However, in this case the amplitude of the dipole is a function of crystal symmetry and sample orientation. Table I gives the form of Γ_{13} for some symmetry/orientation combinations for which D_0 is separable in the fashion stated earlier.

Similar to the 1-D case, consider a cubic system for which Γ_{13} can be separated into two components, one that is purely elastic and one that depends on both thermal and elastic constants (cases 1–4 in Table I). Now consider cases 3a and 3b in detail. The surface normal for these two sample orientations coincides and, hence, experiments corresponding to 3a and 3b can be performed using the same sample. The amplitude of the shear stress dipole for cases 3a and 3b are identical. However, for a sample orientation between case 3a and 3b, the equivalent surface stress is no longer in the form of a shear stress dipole.

Now consider case 4 where the sample has been rotated by some arbitrary angle about the x_2 axis. For case 4, the transformed stresses take the from

$$\begin{aligned} \overline{\sigma}_{13}(\eta, x_3, s) &= -i\eta(C'_{15}\overline{u}_1 + C'_{55}\overline{u}_3) + C'_{55}\overline{u}_{1,3} \\ &\quad + C'_{35}\overline{u}_{3,3}, \\ \overline{\sigma}_{33}(\eta, x_3, s) &= -i\eta(C'_{13}\overline{u}_1 + C'_{35}\overline{u}_3) + C'_{35}\overline{u}_{1,3} \\ &\quad + C'_{33}\overline{u}_{3,3}. \end{aligned} \tag{17}$$

First note that in the rotated coordinate system, C'_{15} and C'_{35} are no longer zero and, as a result, the normal stress does not vanish. Second, the form of the transformed stress does not afford a simple analytical solution contrary to the other cases considered.

III. CONCLUSION

This paper examines the implication of elastic anisotropy as it relates to thermoelastic sources. For the 1-D case, a set of analytical solutions was found for all crystal symmetries/source orientations. These solutions form an appropriate bases set for an angular spectrum of plane waves. For the 2-D case in the limit of strong optical absorption and for specific crystal symmetries and source orientations, a buried line source was shown to be equivalent to applying a shear stress dipole at the bounding surface. However, contrary to the isotropic case, for an arbitrary sample orientation, the equivalent surface normal stress was nonzero and the equivalent surface shear stress was not a simple dipole. This has important implications since the temporal evolution of displacement waveforms is strongly related to the character of the source. For instance, in isotropic materials, displacement waveforms related to laser ablation,[9] which are accurately modeled using a normal point force, are markedly different than waveforms related to thermoelastic generation.[2,9]

ACKNOWLEDGMENTS

The author wishes to express his gratitude to Dr. J. B. Spicer for helpful discussions during the course of this work. This work was sponsored by the U.S. Department of Energy, Office of Science-BES, Materials and Engineering Physics program under DOE Idaho Operations Office Contract No. DE-AC07-99ID13727.

APPENDIX

For the 1D case, N and S are defined as

$$N = \begin{bmatrix} C'_{55}\kappa^2 + \rho s^2 & C'_{45}\kappa^2 & C'_{35}\kappa^2 \\ C'_{45}\kappa^2 & C'_{44}\kappa^2 + \rho s^2 & C'_{34}\kappa^2 \\ C'_{35}\kappa^2 & C'_{34}\kappa^2 & C'_{33}\kappa^2 + \rho s^2 \end{bmatrix},$$

$$S = \begin{bmatrix} i\eta T_0 \beta'_{11}/\sqrt{2\pi}s \\ i\eta T_0 \beta'_{21}/\sqrt{2\pi}s \\ i\eta T_0 \beta'_{31}/\sqrt{2\pi}s \end{bmatrix}. \tag{A1}$$

Since C'_{ij} and β'_{ij} refer to a rotated coordinate system, the set of equations represented by Eq. (6) are valid for all crystal symmetries. In order to elucidate the effect of elastic anisotropy on the source strength, cubic symmetry will be assumed ($\beta_{ij}=\beta_0\delta_{ij}$). This allows the amplitude coefficients to be factored into two terms, one containing both elastic and thermal terms and one containing elastic terms only:

$$\overline{A}_{1j}/T_0\beta_0=\frac{\omega_j^2(C'_{35}C'_{44}\omega_j^2-C'_{45}C'_{34}\omega_j^2-C'_{35}\rho)}{(\kappa_j-\kappa_{r1})(\kappa_j-\kappa_{r2})},$$

$$\overline{A}_{2j}/T_0\beta_0=\frac{\omega_j^2(C'_{34}C'_{55}\omega_j^2-C'_{45}C'_{35}\omega_j^2-C'_{34}\rho)}{(\kappa_j-\kappa_{r1})(\kappa_j-\kappa_{r2})},$$

$$\overline{A}_{3j}/T_0\beta_0=\frac{\omega_j^4(C'^2_{45}-C'_{55}C'_{44})+\omega_j^2\rho(C'_{55}+C'_{44})-\rho^2}{(\kappa_j-\kappa_{r1})(\kappa_j-\kappa_{r2})}, \quad \text{(A2)}$$

$$r_1\neq j,\ \ r_2\neq j,\ \ r_2\neq r_1.$$

For the sake of brevity, N and S for the 2-D problem will be given for case 3 of Table I:

$$N_{11}=C_{11}\eta^2+C_{44}\kappa^2+\rho s^2,\ \ N_{13}=(C_{44}+C_{12})\eta\kappa=N_{31},$$
$$N_{22}=(\eta^2+\kappa^2)C_{44}+\rho s^2,\ \ N_{33}=C_{44}\eta^2+C_{11}\kappa^2+\rho s^2, \quad \text{(A3)}$$

$$N_{12}=N_{21}=N_{23}=N_{32}=0,\ \ S=\begin{bmatrix} i\eta T_0\beta_0/2\pi s \\ 0 \\ i\kappa T_0\beta_0/2\pi s \end{bmatrix}.$$

[1] R. M. White, ''Excitation of Surface Elastic Waves by Transient surface Heating,'' Appl. Phys. Lett. **12**, 12–15 (1963).

[2] C. B. Scruby, R. J. Dewhurst, D. A. Hutchins, and S. B. Palmer, ''Quantitative studies of thermally generated elastic waves in laser-irradiated metals,'' J. Appl. Phys. **51**, 6210–6216 (1980).

[3] D. A. Hutchins and A. C. Tam, ''Pulsed photoacoustic materials characterization,'' IEEE Trans. Ultrason. Ferroelectr. Freq. Control **33**, 439–449 (1986).

[4] L. R. F. Rose, ''Point-source representation for laser-generation ultrasound,'' J. Acoust. Soc. Am. **75**, 723 (1984).

[5] Finite optical penetration and thermal diffusion lead to a precursor spike in the epicentral waveform which can not be accounted for using a stress dipole.

[6] K. L. Telschow and R. J. Conant, ''Optical and thermal parameter effects on laser-generated ultrasound,'' J. Acoust. Soc. Am. **88**, 1494–1502 (1990).

[7] D. H. Hurley, J. B. Spicer, J. W. Wagner, and T. W. Murray, ''Investigation of the anisotropic nature of laser-generated ultrasound in zinc and unidirectional carbon epoxy composites,'' Ultrasonics **36**, 355–360 (1998).

[8] J. R. Bernstein and J. B. Spicer, ''Line source representation for laser-generated ultrasound in aluminum,'' J. Acoust. Soc. Am. **107**, 1352–1357 (2000).

[9] S. J. Davies, C. Edwards, G. S. Taylor, and S. B. Palmer, ''Laser-generated ultrasound: its properties, mechanisms and multifarious applications,'' J. Phys. D **26**, 329–348 (1993).

[10] C. Thomsen, H. T. Grahn, H. J. Maris, and J. Tauc, ''Picosecond interferometric technique for study of phonons in the Brillouin frequency range,'' Opt. Commun. **60**, 55–58 (1986).

[11] G. Tas and H. J. Maris, ''Electron diffusion in metals studied by picosecond ultrasonics,'' Phys. Rev. B **49**, 15046–15054 (1994).

[12] T. Q. Qiu and C. L. Tien, ''Short-pulse laser heating on metals,'' J. Heat Transfer **35**, 719–726 (1992).

[13] V. E. Gusev and O. B. Wright, ''Ultrafast nonequilibrium dynamics of electrons in metals,'' Phys. Rev. B **57**, 2878–2888 (1998).

[14] Typically the lateral dimension of the laser source is much larger than the thickness of the film being investigated.

[15] A. G. Every and W. Sachse, ''Imaging of Laser-Generated Ultrasonic Waves in Silicon,'' in *Acoustical Imaging, Vol. 19*, edited by H. Emert and H.-P. Harjes, (Plenum, New York, 1992), pp. 743–748.

[16] A. Mourad, M. Deschamps, and B. Castagnede, ''Acoustic waves generated by a transient line source in an anisotropic half-space,'' Acustica **82**, 839–851 (1996).

[17] L. Cagniard, *Reflection and Refraction of Prog. Seismic Waves*, (McGraw–Hill, New York, 1962); A. T. de Hoop, Appl. Sci. Res., Sect. B **8**, 349 (1960).

[18] D. H. Hurley and J. B. Spicer, ''Point-source representation for laser-generated ultrasound in an elastic, transversely isotropic half-space,'' J. Appl. Phys. **86**, 3423–3427 (1999).

[19] W. Chen, H. J. Maris, Z. R. Wasilewski, and S. Tamura, ''Attenuation and velocity of 56 GHz longitudinal phonons in gallium arsenide from 50 to 300 K,'' Philos. Mag. B **70**, 687–698 (1994).

[20] O. Matsuda, I. Ishii, T. Fukui, J. J. Baumberg, and O. B. Wright, ''Wavelength selective photoexcitation of picosecond acoustic-phonon pulses in a triple GaAs/$Al_{0.3}Ga_{0.7}$As quantum well structure,'' Physica B **316–317**, 205–208 (2002).

[21] O. B. Wright, B. Perrin, O. Matsuda, and V. E. Gusev, ''Ultrafast carrier diffusion in gallium arsenide probed with picosecond acoustic pulses,'' Phys. Rev. B **64**, 81202-81205 (2001).

[22] The laser source corresponding to Refs. 19–21 was nonthermal.

[23] D. H. Hurley, O. B. Wright, O. Matsuda, V. E. Gusev, and O. V. Kolosov, ''Laser picosecond acoustics in isotropic and anisotropic materials,'' Ultrasonics **38**, 470–474 (2000).

[24] A physical interpretation of this difficulty is easily realized for the case of a source/sink combination in an elastically isotropic material. In this case the image sink and source only produce longitudinal waves and, hence, mode conversion from longitudinal to shear waves at the interface cannot be adequately described with a source and image sink.

[25] J. F. Ready, *Effects of High-Powered Laser Radiation* (Academic, New York, 1971).

[26] The current solution serves as a Green's function which can be used to find the solution due to a distributed source.

[27] It should be noted that by relating $i\omega s$ with the partial derivative with respect to x_1, the remaining integrand is even in ω and hence the integration limits can be changed to the positive ω axis.

[28] R. G. Payton, *Elastic Wave Propagation in Transversely Isotropic Media* (Martinus Nijhoff, The Hague, 1983).

[29] D. H. Hurley, Ph.D. dissertation, Johns Hopkins University, 1997.

[30] B. A. Auld, *Acoustic Fields and Waves in Solids* (Wiley-Interscience, New York, 1973), Vol. 2, pp. 38–43.

[31] M. S. Kharusi and G. W. Farnell, ''Plane ultrasonic transducer diffraction fields in highly anisotropic crystals,'' J. Acoust. Soc. Am. **48**, 665–670 (1970).

[32] J. A. Hildebrand, ''Thermoacoustic generation in anisotropic media,'' J. Acoust. Soc. Am. **79**, 1457–1460 (1985).

[33] In order to correctly account for mode conversion (3-D problem geometry) due to non-normal reflections in isotropic materials, Rose[4] considered a thermoelastic point-source to be buried some distance below the free surface. For an anisotropic half-space, the procedure, presented by Rose, is long and cumbersome owing to the fact that the shear and longitudinal deformations can not be decoupled.